Homogeneous Quenching Immunoassay for Fumonisin B1 Based on Gold Nanoparticles and an Epitope-Mimicking Yellow Fluorescent Protein

Journal:	*ACS Nano*
Manuscript ID	nn-2018-06094x
Manuscript Type:	Article
Date Submitted by the Author:	10-Aug-2018
Complete List of Authors:	Peltomaa, Riikka; Universidad Complutense de Madrid, ANALYTICAL CHEMISTRY Amaro-Torres, Francisco; Universidad Complutense de Madrid, Organic Chemistry Carrasco, Sergio; Universidad Complutense de Madrid, Analytical Chemistry Orellana, Guillermo; Universidad Complutense de Madrid, Organic Chemistry Benito-Peña, Elena; Universidad Complutense de Madrid, Quimica Analitica. Faculty of Chemistry Moreno-Bondi, Maria; Universidad Complutense de Madrid, ANALYTICAL CHEMISTRY

Homogeneous Quenching Immunoassay for Fumonisin B_1 Based on Gold Nanoparticles and an Epitope-Mimicking Yellow Fluorescent Protein

Riikka Peltomaa,[†] Francisco Amaro-Torres,[‡] Sergio Carrasco,[†,⊥] Guillermo Orellana,[‡] Elena Benito-Peña,[,†] and María C. Moreno-Bondi[*,†]*

† Department of Analytical Chemistry and ‡ Department of Organic Chemistry, Chemical Optosensors & Applied Photochemistry Group (GSOLFA), Faculty of Chemistry, Universidad Complutense de Madrid, 28040 Madrid, Spain.

ABSTRACT:

Homogeneous immunoassays represent an attractive alternative due to their simplicity, sensitivity and rapidity. On the basis of a previously identified epitope-mimicking peptide, or mimotope, for fumonisin B_1 (FB_1) mycotoxin, we have developed a homogeneous fluorescence quenching immunoassay based on (17.1 ± 2.0)-nm gold nanoparticles (AuNPs) and a recombinantly produced epitope-mimicking fusion protein. The fumonisin mimotope was cloned as a fusion protein with a yellow fluorescent protein which could be used directly as the tracer for FB_1 detection without the need of labeling or a secondary antibody. Furthermore, owing to the fluorescence quenching ability of AuNPs, a homogeneous immunoassay could be performed

in a single-step without the need of washing steps to separate the unbound tracer. The novel homogeneous assay showed negligible matrix effects in 5% wheat extract and high sensitivity for FB_1 detection, with a dynamic range from 7.3 to 22.6 ng mL^{-1}, a detection limit of 1.1 ng mL^{-1} and IC_{50} value of 12.9 ng mL^{-1} which was significantly lower than the IC_{50} value of the previously reported assay using the synthetic counterpart of the same mimotope in a microarray format. The homogeneous assay was demonstrated to be specific for fumonisins B_1 and B_2, as no significant cross-reactivity with other mycotoxins was observed, and acceptable recoveries (86% for FB_1 2000 µg kg^{-1} and 103% for FB_1 4000 µg kg^{-1} FB1), with RSD < 6.5%, were reported from spiked wheat samples proving that the method could provide a valuable tool for simple analysis of mycotoxin-contaminated food samples.

KEYWORDS: fluorescent protein, mimotope, gold nanoparticle, quenching, homogeneous immunoassay, mycotoxin

Owing to their exceptional optical properties, nanomaterials are often considered ideal for biosensor development and the remarkable progress in the field during the last decades has paved the way for developing ultrasensitive sensors.[1-4] Especially gold nanoparticles (AuNPs) have received particular attention due to their unique optical and electronic properties and, considering their straightforward synthesis, high stability and biocompatibility, high electron density and strong absorption in the visible region, AuNPs continue to be one of the most used materials for different sensing schemes.[5] The latter includes electrochemical,[6] surface-enhanced Raman scattering (SERS),[7] fluorescent[8] and colorimetric assays, as well as other disciplines, such as material sciences, bioimaging and electronics.[1, 9-10] Furthermore, AuNPs are exceptionally

efficient fluorescence quenchers,[11-12] a phenomenon that has been ascribed to various mechanisms, including Förster resonance energy transfer (FRET), nanometal surface energy transfer (NSET),[13-14] and dipole-to-metal particle energy transfer (DMPET).[15-16] Due to the extraordinarily high molar absorption coefficient of AuNPs, broad energy bandwidth, as well as their tunable absorbance according to the nanoparticle size and geometry,[5] AuNPs have been applied as quenchers in fluorescent homogeneous assays[12] based on organic dyes,[17] polymers,[18] quantum dots,[16, 19] as well as fluorescent proteins (FPs).[20]

FPs, which are widely used as markers for gene expression analysis or protein tracking within cells or organelles, and have revolutionized molecular biology in the last decades, are able to emit strong stable fluorescence, and they can be expressed as fusion proteins in recombinant hosts.[21-22] Several FPs with enhanced fluorescence or different spectral characteristics have proven not only their excellence for studying biomolecular interactions but have also further expanded the scope of applications of these proteins, for example for immunoassay development.[23-25] Particularly, FRET-based FP probes have been established as an important tool for studying various intracellular molecules and events,[23] demonstrating the tremendous potential of homogeneous sensing schemes for both *in vivo* and *in vitro* assays where the bound and free tracers can be distinguished without the need of a separation step. Such homogeneous assay formats can result in significant cost and time savings by enabling simpler and faster protocols while, at least theoretically, being more sensitive than the heterogeneous assays.[12, 26]

The exceptional ability of epitope-mimicking peptides, or mimotopes, to imitate the epitope of an antigen and thus bind to same antibody paratope, has been witnessed in several fields including immunotherapy, epitope mapping, and allergy treatment.[27-28] Furthermore, epitope-mimicking peptides and antibodies are an intriguing option to overcome some of the limitations

of competitive immunoassays.[29-30] As they bind to the same antibody paratope as the antigen and elicit a similar antibody response, epitope mimics can be used as the competitor instead of the labeled antigen in applications were the conjugation of the target to a carrier molecule is challenging, or it can cause toxicity to the user. Several mimotopes have been selected from phage-displayed peptide libraries for the detection of low molecular weight targets such as pesticides,[31] neurotoxins,[32] cancer drugs,[33] mycotoxins,[34-36] and other chemicals.[37] Phage-borne peptides have shown great potential for the development of small molecule immunoassays, but considering the large size and the biologically active nature of phages these methods are not always ideal for immunoassay development.[38-39] As an alternative, the synthetic counterparts of the phage-borne mimotopes[40-42] or recombinant peptide-protein fusions,[43-45] have been suggested as phage-free options. Production of recombinant fusion proteins is an attractive alternative because of the low cost of producing recombinant proteins in bacteria and the variety of possibilities to design the protein tailored to the purpose, for example, including tags for purification or using an active enzyme as a fusion protein and later directly as the tracer.[46]

In this work, we present a simple and rapid immunoassay for fumonisin detection based on a recombinant fluorescent fusion protein and fluorescence quenching by AuNPs. Fumonisins are mycotoxins produced by *Fusarium* fungi as secondary metabolites[47] which can be found as natural contaminants commonly in maize, but also in wheat, rice, sorghum, and beans.[48] Owing to the hepatotoxic and carcinogenic effects of fumonisins,[49] as well as the important economic consequences of mycotoxin contamination,[50] detection of these toxins is of great importance. Several international authorities have set regulatory limits, such as the European Commission[51-52] and the United States Food and Drug Administration[53] to ensure food safety. In a previous paper, we have reported the development of a microarray for the detection of fumonisin B_1 (FB_1), the

most abundant and toxic of fumonisins, based on a synthetic mimotope.[40] Here, the FB_1-mimotope is produced recombinantly as a fusion with a yellow fluorescent protein (YFP) which, at the same time, plays as the tracer in the immunoassay. Based on a competitive immunoassay, the YFP-tagged FB_1-mimotope is used as the tracer in a heterogeneous reference assay with immobilized antibody and, furthermore, in a homogeneous quenching assay where the binding event is observed as fluorescence quenching by AuNPs.

RESULTS AND DISCUSSION

Detection of low molecular weight analytes, such as mycotoxins, poses challenges for researchers as direct detection of these molecules is difficult, and the conjugation or labeling needed for the competitive assay format is often challenging. Epitope mimics, which can replace the target conjugate and avoid the use of toxic compounds as assay components, have been described as an intriguing alternative.[30] We have previously identified by phage display an epitope-mimicking peptide, or mimotope, for the fumonisin B_1 (FB_1) mycotoxin.[40] The epitope-mimicking nature of the phage-displayed mimotope was proved in a phage-based immunoassay and, furthermore, the synthetic counterpart of the peptide was used for FB_1 detection in a microarray format. In this work, we further endeavor the possible use of mimotopes by creating a recombinant fusion protein of the same FB_1-mimotope and a YFP. Construction of such fluorescently-tagged mimotope, which can be produced recombinantly in bacteria, allows developing simple immunoassays as neither labeling of the mimotope itself nor secondary antibodies are required. Furthermore, we report the application of the YFP-tagged mimotope to a homogeneous quenching immunoassay that employs AuNPs and enables detection and quantification of FB_1 in a simple, fast, one-step assay.

Construction of the YFP-tagged mimotope. The YFP-tagged FB_1 mimopeptide was generated by cloning the FB_1-mimotope VTPNDDTFDPFR (named A2)[40] in fusion with *Zoanthus sp*. yellow fluorescent protein (YFP), ZsYellow,[54-55] using standard molecular biology techniques. In the mimotope-YFP fusion construct (**Figure 1**), the yellow fluorescent protein and A2-mimotope were separated by a glycine-serine (GS)-linker to ensure sufficient space for the mimotope binding, and a polyhistidine tag (His-tag) downstream of YFP was used to purify the protein by affinity chromatography. To remove the His-tag after purification, a Tobacco Etch Virus (TEV) protease cleavage site was included between the YFP and the His-tag. Successful cleavage was confirmed because the fusion protein no longer binds to the Ni-NTA (nickel-nitrilotriacetic acid) matrix after the TEV-catalyzed reaction. The fluorescent excitation and emission spectra of the purified fluorescent fusion protein is shown in **Figure S1**.

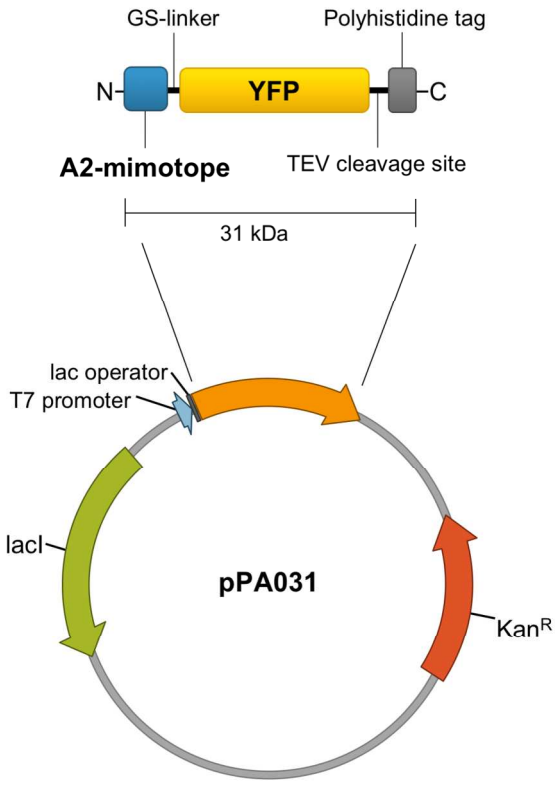

Figure 1. Scheme of the fusion protein construct and main features of the expression vector used for protein production in *E. coli*.

Heterogeneous fluorescence immunoassay. The epitope-mimicking nature of the novel YFP fusion protein and its functionality as a tracer was studied in a heterogeneous fluorescence immunoassay where an anti-FB_1 antibody is immobilized in microtiter wells and competition between FB_1 and the mimotope-YFP is shown as low fluorescence readings in the presence of high FB_1 concentrations (**Figure 2A**). Based on the typical sigmoidal standard curve for a competitive heterogeneous assay (**Figure 2B**) the half maximal inhibitory concentration (IC_{50}) was 6.8 ± 0.3 ng mL^{-1} and the lower limit of detection (LOD), determined as the average signal of the blank minus three times the standard deviation of the blank, turned out to be 3.5 ng mL^{-1}. The dynamic range of the assay, calculated from the IC_{20} and IC_{80} values (**Figure 2B**), was from

3.2 to 14.8 ng mL^{-1}. Although the assay sensitivity was higher than those of the phage-based and synthetic peptide assays,[40] and the assay protocol was simplified because no secondary antibody was needed, the heterogeneous assay still required a few washing steps to remove the unbound reagents and overnight incubation to immobilize the capture antibody.

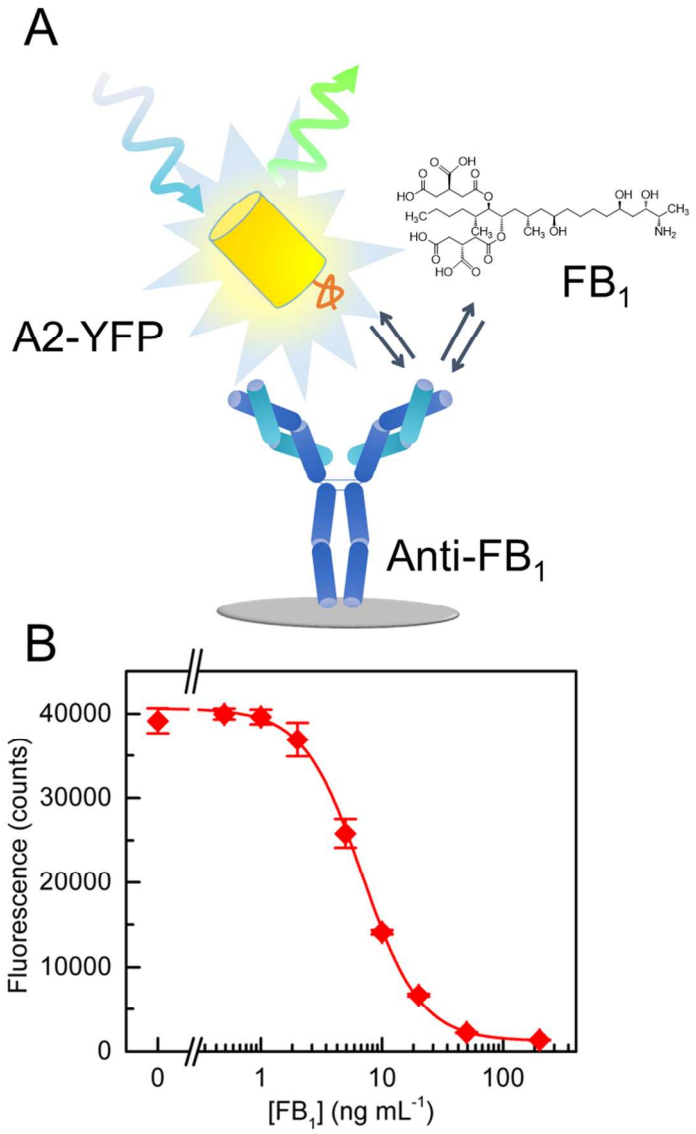

Figure 2. (A) Schematic representation of the heterogeneous fluorescence immunoassay using the mimotope-YFP construct and an immobilized anti-FB_1 antibody. (B) Dose-response curve of the competitive heterogeneous assay. Fluorescence readings (excitation at 500 nm, emission at

545 nm) are depicted as the average of the replicate samples ± the standard error of the mean (n = 3). A four-parameter logistic fit (OriginPro 9.0) was used to calculate the IC values.

Homogeneous quenching immunoassay. The recognition principle of the homogeneous assay is based on fluorescence quenching of the mimotope-YFP construct. As shown in **Figure 3**, the assay uses protein G-coated AuNPs that quench the emission of light upon antibody binding to mimotope-YFP. In the presence of the target FB_1, competition between the latter and the mimotope prevents the fusion protein binding to the antibody and fluorescence is recovered due to the larger distance from the AuNPs. Thus, the one-step assay allows distinguishing the antibody-bound tracer (mimotope-YFP) readily from the free tracer. In addition to the fast and straightforward protocol, the method benefits from the advantage of measuring a signal rise with increasing analyte concentrations in opposition to the heterogeneous reference assay. The low background signal in the absence of the target, due to the strongly quenched fluorescence, makes it easier to detect even small changes in the readout.

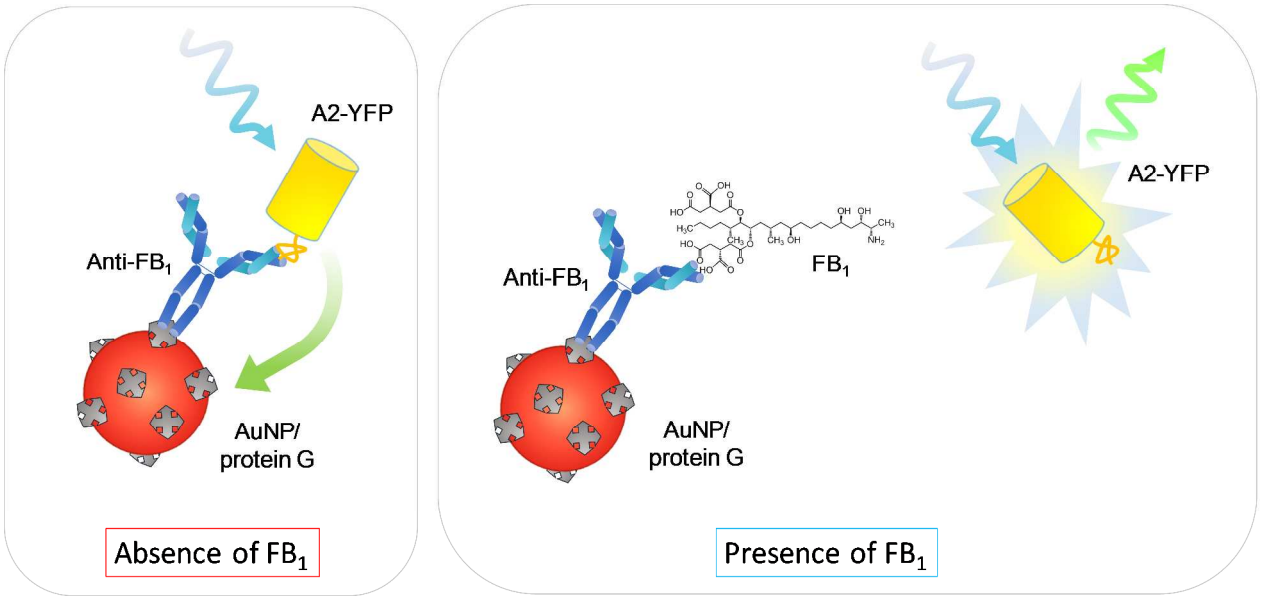

Figure 3. Schematic representation of the homogeneous quenching immunoassay based on the mimotope-YFP and an anti-FB_1 antibody immobilized on AuNP/protein G conjugates. Upon mimotope-YFP binding to the antibody, the AuNP efficiently quenches the intrinsic fluorescence of YFP. In the presence of FB_1, the mimotope-YFP is not bound to the antibody, and its fluorescence is no longer turned off.

Since the efficiency of fluorescence quenching by the AuNP depends not only on the distance from the fluorophore but also on the nanoparticle size,[56] we tested the performance of different AuNPs in the homogeneous quenching immunoassay. Citrate-stabilized gold nanoparticles were prepared by a step-by-step growing procedure,[57] and their average diameters were determined to be (17.1 ± 2.0) nm, (36.1 ± 3.3) nm, and (72.4 ± 7.1) nm by transmission electron microscopy (TEM) (**Figure S2**). The UV-Vis absorption spectra of the AuNPs showed the typical plasmon band peaking at 519 nm, 530 nm and 546 nm for the 17-nm, 36-nm, and 72-nm AuNPs, respectively (**Figure 4**). Furthermore, dynamic light scattering (DLS) was used to evaluate the average hydrodynamic diameter and polydispersity of the nanoparticles (**Figure S3**).

His-tag-mediated conjugation of recombinant protein G to the citrate-capped AuNPs allowed simple, flexible preparation of the protein-decorated AuNPs. Firstly, a flocculation test was performed to determine the amount of protein required to stabilize the AuNPs. Aggregation of bare AuNPs was observed upon addition of 10% (w/v) NaCl, whereas the protein-decorated AuNPs retained their typical plasmon band under the same conditions, confirming a successful protein coating (**Figure S4**). Moreover, the presence of a protein overlayer was observed by TEM (**Figure S5**), and the amount of immobilized protein was determined by hydrolysis and HPLC-analysis (**Figure S6 and Table S1**). AuNPs might also have been directly coupled to

antibodies by non-specific absorption;[58,59] however, protein G-mediated linkage allows a more controlled coupling. Because the antibody is directly added to the assay reaction rather than to the coupling reaction, the exact amount of antibody in the final assay can be determined more precisely, and it is not subject to variations among the different batches prepared. Moreover, in this way, the antibodies would bind to the protein G-coated AuNPs in an oriented manner, ensuring that the antigen binding sites are available and not hindered, which might be (at least partially) the case for non-specifically bound antibodies. Since AuNP-based surface energy transfer (SET) quenching is known to overcome the established distance limits of FRET,[56,60] the additional increase of the distance between AuNPs and the fluorescent protein produced by the protein G overlayer is not as critical as in energy transfer assays based on organic dye acceptors that quench the donors' fluorescence.

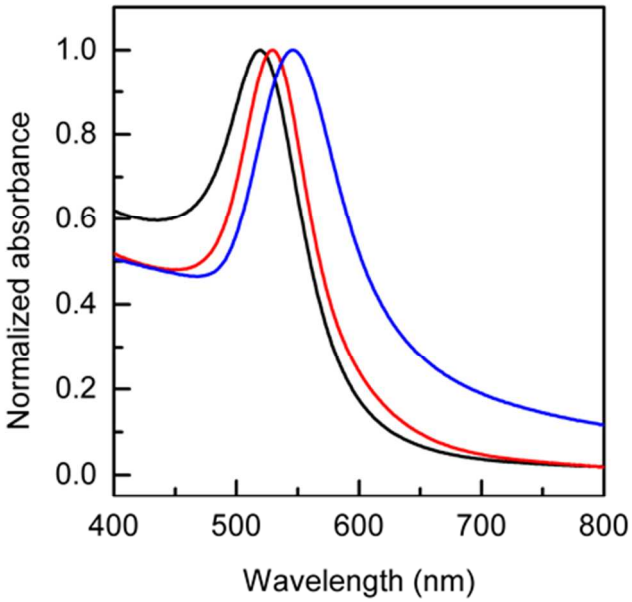

Figure 4. Normalized UV-Vis absorption spectra of the 17-nm (black), 36-nm (red), and 72-nm (blue) AuNPs prepared.

The feasibility of the assay principle was evidenced by observing a strong fluorescence quenching upon the fusion protein binding to the antibody-conjugated AuNPs (Ab-AuNPs). **Figure 5** shows the variation of the mimotope-YFP fluorescence (0.5 μg mL^{-1}) with the concentration of Au-NPs ranging from 0.001 to 4 nM for the 17-nm, 36-nm and 72-nm sizes of the latter. Control experiments in the absence of the nanoparticle-bound antibody (**Figure 5**) confirmed that the fluorescence quenching was predominantly due to the specific binding of the mimotope-YFP to the anti-FB_1 Ab-AuNPs (1.5 μg mL^{-1} of Ab) and not due to the (trivial) phenomena of light scattering, absorption of the excitation light (at 500 nm) and of the fluorescence (at 545 nm) by the Au-NPs themselves. Furthermore, in the presence of 100 ng mL^{-1} FB_1, competition between FB_1 and epitope-mimicking mimotope-YFP resulted in fluorescence signals that were similar to the background levels without the antibody on the nanoparticles.

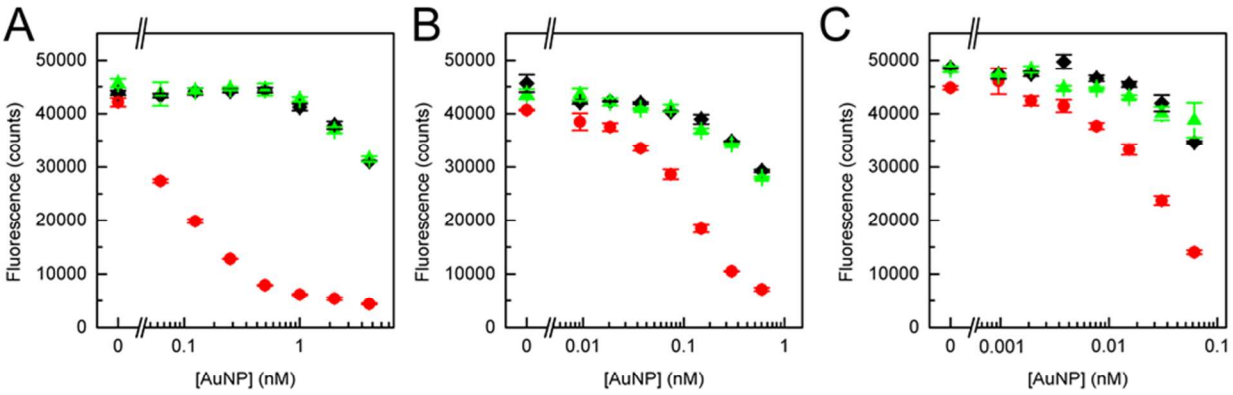

Figure 5. Fluorescence quenching produced by the 17-nm (A), 36-nm (B) and 72-nm (C) AuNPs in the presence of a constant mimotope-YFP concentration of 0.5 μg mL^{-1}. The effect of the AuNP concentration (0.001 – 4 nM) on the fluorescence signal was measured for the antibody-AuNP conjugates (1.5 μg mL^{-1} of Ab) both in the absence (red dots) and in the presence (green

stars) of 100 ng mL^{-1} of FB_1, or without the antibody (black diamonds). The fluorescence signals (excitation at 500 nm, emission at 545 nm) are shown as the average values of replicate samples ± the standard error of the mean (n = 3).

The higher SET efficiency of the smallest Au-NPs of the three sizes tested has been rationalized previously in terms of quenching of the fluorophore occurring within the near field of the AuNP by formation of an image dipole of the former at the nanoparticle surface, once the size-dependent changes in the complex dielectric function and the absorptivity of the AuNPs are factored in.[56] The light scattering effect prevails for nanoparticles larger than 20 nm diameter, effectively decreasing the specific fluorescence quenching by SET. The maximum quenching efficiency (86%), determined from **Figure 5** data as $[1 - (I/I_0)] \times 100$, was obtained with 1 nM 17-nm antibody-decorated particles when 0.5 μg mL^{-1} mimotope-YFP was used. Higher concentrations of AuNPs led to increased levels of quenching even in the absence of FB_1, indicating non-specific binding of mimotope-YFP or rather the effect of the very strong absorption and scattering caused by the AuNPs, taking into account the minimal concentration of the fluorescent molecule. For the larger Au-NPs in particular, the non-specific quenching was observed already at relatively low nanoparticle concentrations (2 pM).

To check the observed maximum efficiency of the nanoparticle SET on the 17-nm AuNPs against the predicted one,[56] we have estimated the distance from the AuNP surface to the YFP chromophore. Taking into account the 3.2 nm protein G coating of the nanoparticle (from TEM, **Figure S5**) supporting the oriented antibody (9.5 nm from top to bottom),[61] and the 4-nm YFP with the chromophore buried approximately in the middle of the protein,[62,63] we can roughly estimate a fluorophore-surface distance of 15 nm. This value assumes that the mimotope has an

insignificant effect. Theory predicts an 86% emission quenching efficiency at 18 nm from the surface of a 16.5 nm (dia.) Au-NP,[56] a value that is very close to the estimated distance considering the approximations involved in our calculation. Furthermore, the efficient SET process between the fluorophore and the AuNP has been shown to be of static nature: single-photon timing fluorescence decay measurements are identical in the absence and in the presence of the antibody-decorated metal nanoparticles (a fluorescence lifetime of 3.60 ± 0.01 ns has been determined for the free and Au-NP-bound mimotope-YFP, **Figure S7**), yet the fluorescence intensity at the detector is *ca.* 6 times larger in the absence of the AuNPs.

For the further assay development, AuNP concentrations with best signal-to-background ratios calculated from maximal and minimal fluorescence signals without or with FB_1, respectively, were selected. To determine the optimum concentrations of mimotope-YFP and the antibody, a checkerboard-type titration was performed with different dilutions. Increasing the mimotope-YFP concentrations obviously resulted in an increase in the fluorescence signals, but high concentrations exhibited also increased non-specific binding in the presence of FB_1 (**Figure S8**). Therefore, 0.5 μg mL^{-1} and 1.5 μg mL^{-1} mimotope-YFP and antibody concentrations, respectively, were chosen for subsequent measurements.

In the homogeneous format, the assay kinetics are usually extremely fast slow diffusion does not limit the rate of the binding reaction to a surface as in heterogeneous assays.[26] In fact, already after 5 min incubation, the specific fluorescence quenching could be observed in our assay (**Figure S9**). Somewhat further increase of the quenching was obtained after 45 min incubation yielding an improved signal-to-background ratio (**Figure S9A**). However, after signal normalization, similar or better sensitivities (expressed as the IC_{50} values) were found with shorter incubation times **(Figure S9B**). Therefore, a 20 min incubation was selected for further

optimization as it provided the required sensitivity but better reproducibility than still shorter incubation times. Then, the specificity of the immunoassay was evaluated by determining the cross-reactivity with other mycotoxins. The assay did not distinguish the structurally related FB_1 and FB_2 fumonisins, since the antibody is not specific to either of the isotopes. Nevertheless, negligible cross-reactivity towards other mycotoxins was observed (**Figure S10**).

On the basis of the optimized conditions, we applied the developed quenching assay to quantification of FB_1 using the various sized AuNPs. Standard FB_1 solutions of different concentrations were mixed with fixed antibody, mimotope-YFP and AuNP concentrations, and after 20 min incubation, the fluorescence of the solutions was measured. **Figure 6A** shows the dose-response plots of the measured signal-to-background fluorescence ratios as a function of the FB_1 concentration. Typical sigmoidal calibration curves were obtained with all the Au-NPs, but the larger the nanoparticle size, the lower the signal-to-background ratio resulted in agreement with the overall effects discussed above.

To investigate the effect of a real sample matrix, the analysis with 17-nm AuNPs was performed in either the assay buffer, i.e. 10 mM phosphate buffer (pH 8.0) containing 0.1% (w/v) BSA, or in wheat extracts diluted with the assay buffer. High concentrations of the sample extract interfered with the assay and resulted in lower maximum signals; however, 5% wheat extract in the final reaction volume showed negligible interference (**Figure 6B**). The calibration curve in this medium showed excellent reproducibility with an average intra-assay RSD (relative standard deviation) of 4.6% and an IC_{50} value of 12.9 ± 1.0 ng mL^{-1}. The assay dynamic range (IC_{20} – IC_{80}) was from 7.3 to 22.6 ng mL^{-1} and its limit of detection (LOD) was calculated to be 1.1 ng mL^{-1}, which was 10-fold better than previously reported with the synthetic peptide,[40] and slightly lower than the heterogeneous reference assay. Others have reported similar and lower

LODs for FB_1 detection (**Table S2**), but the homogeneous quenching assay benefits from significantly shorter assay time and, due to the simple one-step protocol, the method would be ideally suited to multiplexing and automation.

Finally, two wheat samples spiked with FB_1 were analyzed with the homogeneous assay. Sample extracts were diluted in assay buffer, and recoveries of 86% (RSD 6.2%) and 103% (RSD 3.2%) were obtained for samples spiked with 2000 or 4000 μg kg^{-1} FB_1, respectively. Current European regulation on fumonisins covers only maize-based products, and the maximum residue limit for unprocessed maize products is 4000 μg kg^{-1}. Therefore, the novel homogeneous quenching assay might be used as a reliable and accurate method even with real samples.

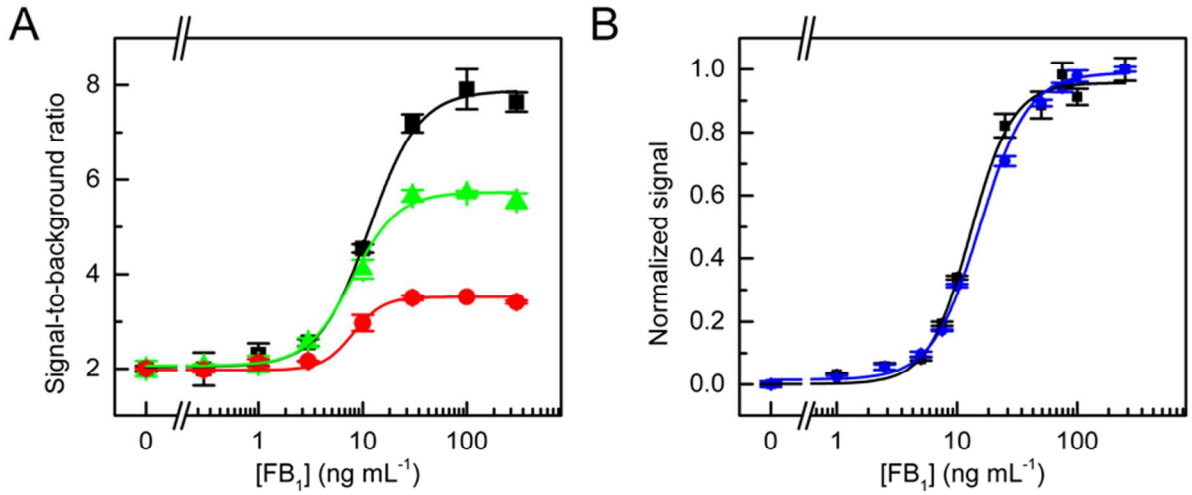

Figure 6. (A) Calibration curves for FB_1 obtained with AuNPs of different sizes: 17 nm (black squares), 36 nm (green triangles) and 72 nm (red dots). Signal-to-background ratios were calculated by dividing the fluorescence in the presence of FB_1 by the signal obtained in the absence of FB_1. (B) Comparison of the dose-response curves in assay buffer (black squares) and in 5% sample extract (blue dots) using 17-nm decorated AuNPs; fluorescence values were

normalized to the mean maximum and minimum absolute signals, and the results are shown as normalized means ± the standard error of the mean (n = 3). Four-parametric logistic fit (OriginPro 9.0) was used to calculate the IC_{50} values.

CONCLUSIONS

This work demonstrates the applicability of epitope mimics to sensitive immunoassays. A novel homogeneous quenching assay for the quantification of FB_1 mycotoxin based on gold NPs demonstrated superior analytical features, including lower detection limit and a more straightforward assay protocol, than the heterogeneous reference assay. Notably, the homogeneous assay based on fluorescent mimotope-YFP fusion protein we have developed is more sensitive than the previously reported immunoassay based on the synthetic mimotope. Because the fluorescent fusion protein was directly used as the tracer, there was no the need for a further labeling reaction or secondary antibodies in contrast to other reported AuNP quenching immunoassays.[17,58] Recombinantly produced fusion proteins guarantee a fixed stoichiometry between the fusion partners, and avoid issues related to batch-to-batch variations or heterogeneous conjugates that are often observed as the product of chemical conjugation reactions. The superb fluorescence quenching efficiency of AuNPs via nanoparticle surface energy transfer is an attractive feature for homogeneous assay development and using His-tag mediated AuNP-coating provides a flexible facile manner to create protein-conjugated AuNPs that can readily be used with different antibodies. Overall, the simplicity and unique capabilities of the quenching assay provides an elaborated yet powerful new tool for rapid analysis of mycotoxins in food samples.

EXPERIMENTAL SECTION

Materials. pZsYellow vector was obtained from Clontech Laboratories (Mountain View, CA) while the expression vector pQE-T2-2 together with the Ni-NTA (nickel–nitrilotriacetic acid) magnetic agarose beads were from Qiagen (Hilden, Germany). Chemically competent *Escherichia coli* One Shot® BL21 Star™ (DE3) cells, Phusion HF DNA polymerase, restriction enzymes, and Pierce™ BCA protein assay kit were from Thermo Fisher Scientific (Waltham, MA). Oligonucleotides were obtained from Integrated DNA Technologies (San Diego, CA). HisTrap FF and PD-10 columns were from GE Healthcare (Little Chalfont, UK). Bacterial cell lysis buffer and bovine serum albumin (BSA) were purchased from NZYTech (Lisbon, Portugal). Amicon Ultra Centrifugal filters were from Merck Millipore (Burlington, MA) and Packard HTRF 96-well black plates from Nunc (Roskilde, Denmark). Protease inhibitor cocktail and TEV protease, together with sodium citrate (+99%) and tetrachloroauric(III) acid trihydrate ($HAuCl_4 \cdot 3H_2O$, +99.9%) were purchased from Sigma-Aldrich (St. Louis, MO). Recombinant protein G with His-tag was obtained from Abcam (Cambridge, UK).

Monoclonal anti-fumonisin antibody was purchased from BioTez (Berlin, Germany). Mycotoxins fumonisin B_1 (FB_1), fumonisin B_2 (FB_2), T-2 toxin, and HT-2 toxin were from Fermentek (Jerusalem, Israel); alternariol (AOH) was from Apollo Scientific (Bredbury, UK), while deoxynivalenol (DON) and zearalenone (ZEA) were from Sigma-Aldrich. The blank wheat quality control material was purchased from Romer laboratories (Getzersdorf, Austria).

Construction of fluorescent fusion proteins. For the expression of YPF-tagged mimotope A2, plasmid pPA031 was constructed. The ZsYellow gene was PCR-amplified from vector pZsYellow by Phusion HF DNA polymerase with oligonucleotides RP08Fw and PA09Rv. The sense primer RP08Fw (5'–TTC GAG CTC ATG GTT ACT CCG AAT GAT GAT ACG TTT

GAT CCT TTT CGG GGT GGA GGT TCG GCT CAT TCA AAG CAC GGT CTA–3') contained a 5'-overhang composed of the DNA sequence encoding for the mimotope A2 (underlined) to generate the translational fusion A2-YFP. The antisense primer PA09Rv (5'–GCT GGT ACC TGG CCC TGA AAA TAC AGG TTT TCG GCC AAG GCA GAA GGG AAT GC–3'), hybridizing to the 3'-end of the *ZsYFP*, was used to add a TEV cleavage site between the 10xHis-tag and the C-terminus of YFP. The PCR product was subcloned at the SacI and KpnI sites of pQE-T7-2 to generate pPA031. Successful cloning was confirmed by DNA sequence analysis.

Fusion protein expression and purification. For the overexpression of the mimotope-YFP fusion protein, plasmid pPA031 was transformed into *E. coli* One Shot® BL21 Star™ (DE3) cells and selected on LB agar plates with 50 μg/mL kanamycin. A single colony harboring the plasmid was used to inoculate 15 mL preculture (LB medium supplemented with 50 μg/mL kanamycin), which was grown overnight at +30 °C. The cells growth was spectrophotometrically monitored, and, the following day, preculture in the exponential growth phase was used to inoculate a main culture of 250 mL (LB medium supplemented with 50 μg/mL kanamycin) to an optical density at 600 nm (OD_{600}) of 0.05. The main culture was grown at 37 °C with shaking until an OD_{600} of 0.6 was reached, and IPTG (isopropyl β-D-1-thiogalactopyranoside) was added to a final concentration of 500 μM to induce fusion protein expression. The cultivation was then continued at 37 °C for 5 h. After that, the cells were collected by centrifugation (10 min at 5000g at +4 °C) and resuspended in 10 mL of lysis buffer supplemented with protease inhibitor cocktail. The cells were lysed by sonication on ice for 3 min, after which the resultant cell debris was removed by centrifugation for 20 min at 15,000g at +4 °C. Successful expression of the

fluorescent protein was confirmed by analyzing the fluorescence emission of the soluble and insoluble fractions as well as the culture media.

The fluorescent fusion protein was purified from the cell lysate by HisTrap column according to manufacturer's instructions. First, the clarified lysate was diluted (1:3 v/v) in binding buffer (20 mM phosphate buffer pH 7.2, 500 mM NaCl and 20 mM imidazole) to ensure optimal binding conditions for the purification. After loading the sample in the HisTrap column, the latter was washed with 30 mL of the binding buffer and, finally, the His-tagged proteins were eluted by elution buffer (20 mM phosphate buffer pH 7.2, 500 mM NaCl and 500 mM imidazole). Presence of the fluorescent protein in the elution fractions was followed spectrophotometrically and the fluorescent fractions were pooled. The buffer was exchanged to 50 mM Tris buffer (pH 7.75) containing 150 mM NaCl with PD-10 according to manufacturer's instructions and concentrated using Amicon Ultra 3K Centrifugal Filter Units. The concentration of the stock was determined by BCA kit, and to remove the C-terminal His-tag, 4 μg of TEV protease was added to 100 μg of the fusion protein (in 100 μL of 50 mM Tris buffer pH 7.75 containing 150 mM NaCl). After an overnight incubation at +4 °C, the cleaved His-tag and the His-tagged TEV protease were removed by adding 50 μL of Ni-NTA magnetic agarose beads to the reaction. The beads were captured with a Nd magnet after 15 min and the supernatant was collected. Successful His-tag cleavage was confirmed by observing the fluorescence emission in the fraction which did not bind to Ni-NTA beads. Finally, protein concentration of the purified mimotope-YFP without His-tag was determined with a BCA assay kit and its purity was verified by SDS-PAGE. The fluorescent excitation and emission spectra of the purified fluorescent fusion protein is shown in **Figure S1**.

Heterogeneous fluorescence immunoassay. The heterogeneous fluorescence immunoassay with mimotope-YFP (**Figure 2A**) was performed in 96-well black plates by coating the wells with capture antibody (100 ng in 60 μL of 0.2 M sodium carbonate/bicarbonate, pH 9.4) by overnight incubation at +4 °C. The wells were then blocked with blocking buffer (PBS pH 7.2; 3% (w/v) BSA) for 3 h at room temperature and washed twice with PBS-T (PBS pH 7.2; 0.05% (v/v) Tween-20). Toxin standards in the range of 0 to 250 ng mL^{-1} (in three replicates) were added to the coated wells together with the 1 μg mL^{-1} mimotope-YFP in assay buffer (PBS, pH 7.2; 0.05% (v/v) Tween-20; 0.1% (w/v) BSA) in a total reaction volume of 60 μL. After incubation of 1.5 h at slow shaking, the wells were washed four times with PBS-T. Finally, 60 μL of PBS was added to each well and fluorescence signals (excitation at 500 nm; detection at 545 nm) were measured using a BMG Labtech (Ortenberg, Germany) CLARIOstar microplate reader.

Gold nanoparticle (AuNP) synthesis and characterization. The effect of the gold nanoparticles size on the fluorescence quenching was evaluated by preparing the metal colloids following a step-by-step growing procedure described elsewhere,[57] with minor modifications. Firstly, 97 mg (0.33 mmol) of trisodium citrate dihydrate was dissolved in 150 mL Milli-Q water (used immediately after collection from the system, 18.2 MΩcm at 25 °C, pH 7.33) in a 250 mL two-necked round-bottom flask attached to a condenser. A 25 mM $HAuCl_4$ stock solution was prepared by dissolving 246 mg of gold(III) chloride trihydrate in 25 mL of Milli-Q water. Once the solution containing sodium citrate boiled (110 °C), 1 mL of the gold solution was rapidly injected under vigorous stirring, obtaining in this way citrate-capped AuNPs after ca. 10 min. The reaction mixture was cooled to +90 ºC and two consecutive injections of 1 mL $HAuCl_4$ solution were performed every 30 min. Then, 30 min after the second addition, 55 mL of the

suspension was extracted, centrifuged (at 12857 g for 2 h) and re-suspended into the same amount of Milli-Q water to yield the 'generation 0' (Gen0) suspension. Then, 53 mL of Milli-Q water was added to the remaining mixture in the round-bottom flask and kept under stirring for 15 min until the temperature reached +90 °C. Separately, a 60 mM sodium citrate stock solution was prepared (441 mg in 25 mL of Milli-Q water), and 2 mL of this stock solution was added to the reaction mixture to yield the seed solution for the following generation. In this case, three consecutive injections of 1 mL $HAuCl_4$ solution were incorporated at 30 min intervals. After 30 min of the third addition, 55 mL of the suspension was extracted and treated as described previously to obtain 'generation 1' (Gen1). The procedure was repeated in an iteratively fashion until 'generation 6' (Gen6) was reached. For the assay optimization, samples of Gen0, Gen3, and Gen6, corresponding to 17-nm, 36-nm and 72-nm nanoparticles, respectively, were used.

TEM images were acquired using a JEOL JEM-1400PLUS instrument operating at 120 kV, with a LaB_6 electron source and a GATAN US1000 CCD camera (2k × 2k). The diameter of at least 150 particles was determined from these TEM images using ImageJ software (National Institutes of Health, US) to characterize the size distribution of the nanoparticles. The absorption spectra of the AuNPs were measured on a Varian Cary 3-Bio UV-Vis spectrophotometer. Their concentration was determined from the UV-Vis spectra using the reported absorption coefficients at 450 nm (ε_{450}) for AuNPs of different sizes,[64] namely 3.24×10^8 M^{-1} cm^{-1}, 3.52×10^9 M^{-1} cm^{-1}, and 2.93×10^{10} M^{-1} cm^{-1} for 17-nm, 36-nm, and 72-nm AuNPs, respectively. Hydrodynamic diameter and zeta potential measurements were conducted on a CGS-8 (ALV, Hessen, Germany) instrument equipped with an Ar-ion laser (Coherent I300, 514.5 nm).

Recombinant protein G with HisTag was conjugated to citrate-stabilized AuNPs as previously described with minor modifications.[65] Initially, the protein concentration required to stabilize

AuNPs was tested by flocculation tests with NaCl.[59] Briefly, 150 μL AuNPs (2.5 nM) and different concentrations (0–7.8 μg mL^{-1}) of protein G in 10 mM phosphate buffer (pH 8.0) were mixed in a AuNP/protein mole ratio ranging from 1:0 to 1:120). After 15 min incubation at room temperature, 50 μL of 10% NaCl solution was added to the above mixture and the stability of the gold was monitored by its color and by the absorbance of the mixture. Based on the flocculation test, for the self-assembly of the AuNP-protein G conjugates, 6.5 μg mL^{-1} (250 nM) protein G was added to an Eppendorf tube containing a AuNP suspension (2.5 nM of 17-nm AuNPs, 0.4 nM of 26-nm AuNPs, or 0.04 nM of 72-nm AuNPs) in 10 mM phosphate buffer (pH 8.0). After incubation for 45 min at +4 °C, the suspension was washed twice by centrifugation at 12000g for 20 min and, finally, the AuNP-protein G conjugates were resuspended in 10 mM phosphate buffer (pH 8.0) with 0.1% (w/v) BSA, using 1/10 of the original reaction volume to achieve stocks of a higher concentration. Quantification of the protein G coverage was performed by hydrolysis of the protein immobilized onto the AuNPs and classical amino acid HPLC analysis of the hydrolysates, following the strategy described by Liu *et al*. (2017) [66] (see supporting information for method details).

Homogeneous quenching immunoassay. The homogeneous quenching immunoassay with mimotope-YFP plus protein G-coupled AuNPs (**Figure 4**) was performed in 96-well black plates in one step by mixing the assay components in 10 mM phosphate buffer (pH 8.0) containing 0.1% (w/v) BSA in a total reaction volume of 60 μL. After a checkerboard-type titration of the antibody and mimotope-YFP to determine their optimal concentrations, 1.5 μg mL^{-1} anti-FB_1 antibody and 0.5 μg mL^{-1} mimotope-YFP were used and mixed with the toxin standards in the 0-250 ng mL^{-1} range (in three replicates). For the optimization of AuNP-protein G conjugates, concentrations ranging from 0.001 to 4 nM were studied but, for the calibration curves, 1 nM

(17-nm AuNP), 0.6 nM (36-nm AuNPs), or 0.06 nM (72-nm AuNPs) concentrations were used. After 10–45 min incubation at room temperature, fluorescence (excitation at 500 nm; detection at 545 nm) was measured using the CLARIOstar microplate reader.

Sample preparation and analysis of spiked samples. A blank wheat reference material was used to confirm the functionality of the homogeneous assay with a real sample matrix. According to a previously described protocol for FB_1 extraction,[43] 5 g of the blank wheat sample was suspended in 25 mL of PBS or, for the spiked samples, 2 or 4 μg of FB_1 was added to 1 g of wheat suspended in 5 mL of PBS (2000 or 4000 μg kg^{-1} of FB_1). Suspensions were ultrasonically extracted for 15 min and centrifuged at 15000 g for 15 min. The supernatant was filtered with a 0.22 μm nylon filter to remove any insoluble material and diluted in the assay buffer.

Data analysis. For the toxin dose-response plots, **t**he fluorescence signals were analyzed with OriginPro 9.0 software (OriginLab Corp., Northampton, MA) using a four-parameter logistic regression (4-PL) function (**eq 1**),

$$y = A_{min} + \frac{(A_{max} - A_{min})}{1 + \left(\frac{x}{IC_{50}}\right)^{b}} \qquad (1)$$

where A_{max} is the asymptotic maximum, b and IC_{50} are the slope of the curve and the analyte concentration, respectively, at the inflection point, and A_{min} is the asymptotic minimum. The limit of detection (LOD) was determined using the average blank signal ± 3× the standard deviation of the blank, while the dynamic range of the assay was defined as that corresponding to the 20% to 80% inhibition ($IC_{20} - IC_{80}$).

ASSOCIATED CONTENT

Supporting Information.

Supporting information is available free of charge on the ACS Publications website, and it includes excitation and emission spectra of the purified fluorescent fusion protein, characterization of the gold nanoparticles (AuNPs) by transmission electron microscopy (TEM) and dynamic light scattering (DLS), as well as characterization of the protein G-coated AuNPs and optimization of the homogeneous quenching immunoassay plus cross-reactivity studies. Supplementary Table 2 includes comparison of the reported method with other known assays for FB_1 detection.

AUTHOR INFORMATION

Corresponding Authors

* María Cruz Moreno-Bondi and Elena Benito-Peña. Department of Analytical Chemistry, Faculty of Chemistry, Universidad Complutense de Madrid, Av. Complutense, s/n, 28040 Madrid, Spain. E-mail: mcmbondi@ucm.es and elenabp@ucm.es, Tel: +34-91 394 5147, Fax: 34-91 394 4329.

Present Addresses

⊥ Department of Organic Chemistry, Stockholm University, Stockholm 10691, Sweden

Author Contributions

The manuscript was written through contributions of all authors. All authors have given approval to the final version of the manuscript.

Funding Sources

This study was supported by the Ministry of Economy and Competitiveness (MINECO, CTQ2015-69278-C2). R.P. acknowledges UCM for a predoctoral grant.

Notes

The authors declare no competing financial interest.

ABBREVIATIONS

AuNP, gold nanoparticle; FB_1, fumonisin B_1; FP, fluorescent protein; YFP, yellow fluorescent protein; LOD, limit of detection; IC_{50} half maximal inhibitory concentration.

REFERENCES

1. Howes, P. D.; Chandrawati, R.; Stevens, M. M., Colloidal Nanoparticles as Advanced Biological Sensors. *Science* **2014,** *346*, 1247390.
2. Holzinger, M.; Le Goff, A.; Cosnier, S., Nanomaterials for Biosensing Applications: A Review. *Front. Chem.* **2014,** *2*, 63.
3. De, M.; Ghosh, P. S.; Rotello, V. M., Applications of Nanoparticles in Biology. *Adv. Mater.* **2008,** *20*, 4225–4241.
4. Lei, J.; Ju, H., Signal Amplification Using Functional Nanomaterials for Biosensing. *Chem. Soc. Rev.* **2012,** *41*, 2122–2134.
5. *Encyclopedia of Metalloproteins*. Kretsinger, R. H.; Uversky, V. N.; Permyakov, E. A. Eds.; Springer: New York, 2013.
6. Guo, S.; Dong, S., Biomolecule-Nanoparticle Hybrids for Electrochemical Biosensors. *Trends Anal. Chem.* **2009,** *28*, 96–109.
7. Porter, M. D.; Lipert, R. J.; Siperko, L. M.; Wang, G.; Narayanan, R., SERS as a Bioassay Platform: Fundamentals, Design, and Applications. *Chem. Soc. Rev.* **2008,** *37*, 1001–1011.
8. Deng, W.; Goldys, E. M., Plasmonic Approach to Enhanced Fluorescence for Applications in Biotechnology and the Life Sciences. *Langmuir* **2012,** *28*, 10152–10163.
9. Saha, K.; Agasti, S. S.; Kim, C.; Li, X.; Rotello, V. M., Gold Nanoparticles in Chemical and Biological Sensing. *Chem. Rev.* **2012,** *112*, 2739–2779.
10. Bazin, I.; Andreotti, N.; Hassine, A. I.; De Waard, M.; Sabatier, J. M.; Gonzalez, C., Peptide Binding to Ochratoxin A mycotoxin: A New Approach in Conception of Biosensors. *Biosens. Bioelectron.* **2013,** *40*, 240–246.
11. *FRET – Förster Resonance Energy Transfer. From Theory to Applications*. Medintz, I. L.; Hildebrandt, N. Eds.; Wiley-VCH: Weinheim, Germany, 2014.
12. Sapsford, K. E.; Berti, L.; Medintz, I. L., Materials for Fluorescence Resonance Energy Transfer Analysis: Beyond Traditional Donor-Acceptor Combinations. *Angew. Chem. Int. Ed.* **2006,** *10*, 4562–4589.
13. Jennings, T. L.; Singh, M. P.; Strouse, G. F., Fluorescent Lifetime Quenching near d = 1.5 nm Gold Nanoparticles: Probing NSET Validity. *J. Am. Chem. Soc.* **2006,** *128*, 5462–5467.
14. Yun, C. S.; Javier, A.; Jennings, T.; Fisher, M.; Hira, S.; Peterson, S.; Hopkins, B.; Reich, N. O.; G.F., S., Nanometal Surface Energy Transfer in Optical Rulers, Breaking the FRET Barrier. *J. Am. Chem. Soc.* **2005,** *127*, 3115–3119.

15. Carminati, R.; Greffet, J. J.; Henkel, C.; Vigoureux, J. M., Radiative and Non-Radiative Decay of a Single Molecule Close to a Metallic Nanoparticle. *Opt. Commun.* **2006,** *261*, 368–375.
16. Pons, T.; Medintz, I. L.; Sapsford, K. E.; Higashiya, S.; Grimes, A. F.; English, D. S.; Mattoussi, H., On the Quenching of Semiconductor Quantum Dot Photoluminescence by Proximal Gold Nanoparticles. *Nano Lett.* **2007,** *7*, 3157–3164.
17. Mayilo, S.; Ehlers, B.; Wunderlich, M.; Klar, T. A.; Josel, H. P.; Heindl, D.; Nichtl, A.; Kürzinger, K.; Feldmann, J., Competitive Homogeneous Digoxigenin Immunoassay Based on Fluorescence Quenching by Gold Nanoparticles. *Anal. Chim. Acta* **2009,** *646*, 119–122.
18. You, C. C.; Miranda, O. R.; Gider, B.; Ghosh, P. S.; Kim, I. B.; Erdogan, B.; Krovi, S. A.; Bunz, U. H.; Rotello, V. M., Detection and Identification of Proteins Using Nanoparticle-Fluorescent Polymer 'Chemical Nose' Sensors. *Nat. Nanotechnol.* **2007,** *2*, 318–232.
19. Qian, J.; Wang, C.; Pan, X.; Liu, S., A High-throughput Homogeneous Immunoassay Based on Förster Resonance Energy Transfer between Quantum Dots and Gold Nanoparticles. *Anal. Chim. Acta* **2013,** *763*, 43–49.
20. De, M.; Rana, S.; Akpinar, H.; Miranda, O. R.; Arvizo, R. R.; Bunz, U. H.; Rotello, V. M., Sensing of Proteins in Human Serum Using Conjugates of Nanoparticles and Green Fluorescent Protein. *Nat. Chem.* **2009,** *1*, 461–465.
21. Schmid, J. A.; Neumeier, H., Evolutions in Science Triggered by Green Fluorescent Protein (GFP). *Chembiochem* **2005,** *6*, 1149–1156.
22. Tsien, R. Y., The Green Fluorescent Protein. *Annu. Rev. Biochem.* **1998,** *67*, 509–544.
23. Tamura, T.; Hamachi, I., Recent Progress in Design of Protein-Based Fluorescent Biosensors and Their Cellular Applications. *ACS Chem. Biol.* **2014,** *9*, 2708–2717.
24. Chung, C.; Makino, R.; Ohmuro-Matsuyama, Y.; Ueda, H., Development of a Fluorescent Protein-Antibody Förster Resonance Energy Transfer Probe for the Detection and Imaging of Osteocalcin. *J. Biosci. Bioeng.* **2017,** *23*, 272–276.
25. Sakamoto, S.; Taura, F.; Pongkitwitoon, B.; Putalun, W.; Tsuchihashi, R.; Kinjo, J.; Tanaka, H.; Morimoto, S., Development of Sensitivity-Improved Fluorescence-Linked Immunosorbent Assay Using a Fluorescent Single-Domain Antibody against the Bioactive Baphthoquinone, Plumbagin. *Anal. Bioanal. Chem.* **2010,** *396*, 2955–2963.
26. *The Immunoassay Handbook: Theory and applications of ligand binding, ELISA and related techniques*. Wild, D. E. Eds.; Elsevier Ltd.: Oxford, UK, 2013.
27. Luzar, J.; Štrukelj, B.; Lunder, M., Phage Display Peptide Libraries in Molecular Allergology: From Epitope Mapping to Mimotope-Based Immunotherapy. *Allergy* **2016,** *71*, 1526-1532.
28. Wai, C. Y. Y.; Leung, N. Y. H.; Leung, P. S. C.; Chu, K. H., Immunotherapy of Food Allergy: A Comprehensive Review. *Clin. Rev. Allergy Immunol.* **2017**.
29. Chauhan, R.; Singh, J.; Sachdev, T.; Basu, T.; Malhotra, B. D., Recent Advances in Mycotoxins Detection. *Biosens. Bioelectron.* **2016,** *81*, 532–545.
30. Peltomaa, R.; Benito-Peña, E.; Moreno-Bondi, M. C., Bioinspired Recognition Elements for Mycotoxin Sensors. *Anal. Bioanal. Chem.* **2018,** *410*, 747–771.
31. Zhao, F.; Wang, H.; Han, X.; Yang, Z., Development and Comparative Study of Chemosynthesized Antigen and Mimotope-Based Immunoassays for Class-Specific Analysis of O,O-Dimethyl Organophosphorus Pesticides. *Sci. Rep.* **2016,** *22*, 37640.

32. Gazarian, T.; Selisko, B.; Hérion, P.; Gazarian, K., Isolation and Structure-Functional Characterization of Phage Display Library-Derived Mimotopes of Noxiustoxin, a Neurotoxin of the Scorpion *Centruroides noxius* Hoffmann. *Mol. Immunol.* **2000,** *37*, 755–766.
33. Liu, J.; Chisti, M. M.; Zeng, X., General Signal Amplification Strategy for Nonfaradic Impedimetric Sensing: Trastuzumab Detection Employing a Peptide Immunosensor. *Anal. Chem.* **2017,** *89*, 4013–4020.
34. Wang, Y.; Wang, H.; Li, P.; Zhang, Q.; Kim, H. J.; Gee, S. J.; Hammock, B. D., Phage-Displayed Peptide That Mimics Aflatoxins and Its Application in Immunoassay. *J. Agric. Food Chem.* **2013,** *61*, 2426–2433.
35. He, Z. Y.; He, Q. H.; Xu, Y.; Li, Y. P.; Liu, X.; Chen, B.; Lei, D.; Sun, C. H., Ochratoxin A Mimotope from Second-Generation Peptide Library and Its Application in Immunoassay. *Anal. Chem.* **2013,** *85*, 10304–10311.
36. He, Q.-h.; Xu, Y.; Zhang, C.-z.; Li, Y.-p.; Huang, Z.-b., Phage-Borne Peptidomimetics as Immunochemical Reagent in Dot-Immunoassay for Mycotoxin Zearalenone. *Food Control* **2014,** *39*, 56–61.
37. Wang, J.; Liu, Z.; Li, G.; Li, J.; Kim, H. J.; Shelver, W. L.; Li, Q. X.; Xu, T., Simultaneous Development of Both Competitive and Noncompetitive Immunoassays for 2,2′,4,4′-Tetrabromodiphenyl Ether using Phage-Displayed Peptides. *Anal. Bioanal. Chem.* **2013,** *405*, 9579–9583.
38. Smartt, A. E.; Ripp, S., Bacteriophage Reporter Technology for Sensing and Detecting Microbial Targets. *Anal. Bioanal. Chem.* **2011,** *400*, 991–1007.
39. Peltomaa, R.; López-Perolio, I.; Benito-Peña, E.; Barderas, R.; Moreno-Bondi, M. C., Application of Bacteriophages in Sensor Development. *Anal. Bioanal. Chem.* **2016,** *408*, 1805–1828.
40. Peltomaa, R.; Benito-Peña, E.; Barderas, R.; Sauer, U.; Gonzalez Andrade, M.; Moreno-Bondi, M. C., Microarray-Based Immunoassay with Synthetic Mimotopes for the Detection of Fumonisin B_1. *Anal. Chem.* **2017,** *89*, 6216–6223.
41. Zou, X.; Chen, C.; Huang, X.; Chen, X.; Wang, L.; Xiong, Y., Phage-Free Peptide ELISA for Ochratoxin A Detection Based on Biotinylated Mimotope as a Competing Antigen. *Talanta* **2016,** *146*, 394–400.
42. Liu, R.; Yu, Z.; He, Q.; Xu, Y., An Immunoassay for Ochratoxin A without the Mycotoxin. *Food Control* **2007,** *18*, 872–877.
43. Xu, Y.; Chen, B.; He, Q. H.; Qiu, Y. L.; Liu, X.; He, Z. Y.; Xiong, Z. P., New Approach for Development of Sensitive and Environmentally Friendly Immunoassay for Mycotoxin Fumonisin B_1 Based on Using Peptide-MBP Fusion Protein as Substitute for Coating Antigen. *Anal. Chem.* **2014,** *86*, 8433–8440.
44. Xu, Y.; He, Z.; He, Q.; Qiu, Y.; Chen, B.; Chen, J.; Liu, X., Use of Cloneable Peptide-MBP Fusion Protein as a Mmetic Coating Antigen in the Standardized Immunoassay for Mycotoxin Ochratoxin A. *J. Agric. Food Chem.* **2014,** *62*, 8830–8836.
45. Carlomagno, M.; Lassabe, G.; Rossotti, M.; González-Techera, A.; Vanrell, L.; González-Sapienza, G., Recombinant Streptavidin Nanopeptamer Anti-Immunocomplex Assay for Noncompetitive Detection of Small Analytes. *Anal. Chem.* **2014,** *86*, 10467–10473
46. Ding, Y.; Hua, X.; Chen, H.; Liu, F.; González-Sapien, G.; Wang, M., Recombinant Peptidomimetic-Nano Luciferase Tracers for Sensitive Single-Step Immunodetection of Small Molecules. *Anal. Chem.* **2018,** *90*, 2230–2237.

47. Gelderblom, W. C.; Jaskiewicz, K.; Marasas, W. F.; Thiel, P. G.; Horak, R. M.; Vleggaar, R.; Kriek, N. P., Fumonisins - Novel Mycotoxins with Cancer-Promoting Activity Produced by *Fusarium moniliforme*. *Appl. Environ. Microbiol.* **1988,** *54*, 1806–1811.
48. Scott, P. M., Recent Research on Fumonisins: A Review. *Food Addit. Contam., Part A* **2012,** *29*, 242–248.
49. IARC, International Agency for Research on Cancer (2002) Fumonisin B1, in: IARC monographs on the evaluation of the carcinogenic risks to humans: Some traditional herbal medicines, some mycotoxins, naphthalene and styrene, vol. 82. IARC, Lyon, France, pp 301–366.
50. Bennett, J. W.; Klich, M., Mycotoxins. *Clin. Microbiol. Rev.* **2003,** *16*, 497–516.
51. European Commission. Commission regulation (EC) 1881/2006. Off J Eur Union. L364:5–24.
52. European Commission. Commission regulation (EC) 1126/2007. Off J Eur Union. 2007; L255:14-17.
53. US Food and Drug Administration (FDA), Draft guidance for industry: Fumonisin levels in human food and animal feeds; final guidance. (http://www.fda.gov/food/guidanceregulation/guidancedocumentsregulatoryinformation/ucm109231.htm). [Cited 10 May 2018].
54. Matz, M. V.; Fradkov, A. F.; Labas, Y. A.; Savitsky, A. P.; Zaraisky, A. G.; Markelov, M. L.; Lukyanov, S. A., Fluorescent Proteins from Nonbioluminescent *Anthozoa* Species. *Nat. Biotechnol.* **1999,** *17*, 969–973.
55. Clontech (2002) Living colors user manual, vol II. Red fluorescent protein, protocol PT3404-1. www.clontech.com. [Cited 10 May 2018].
56. Breshike, C. J.; Riskowski, R. A.; Strouse, G. F., Leaving Förster Resonance Energy Transfer Behind: Nanometal Surface Energy Transfer Predicts the Size-Enhanced Energy Coupling between a Metal Nanoparticle and an Emitting Dipole. *J. Phys. Chem. C.* **2013,** *117*, 23942–23949.
57. Bastus, N. G.; Comenge, J.; Puntes, V., Kinetically Controlled Seeded Growth Synthesis of Citrate-Stabilized Gold Nanoparticles of up to 200 nm: Size Focusing versus Ostwald Ripening. *Langmuir* **2011,** *27*, 11098–11105.
58. Chen, J.; Huang, Y.; Zhao, S.; Lu, X.; Tian, J., Gold Nanoparticles-Based Fluorescence Resonance Energy Transfer for Competitive Immunoassay of Biomolecules. *Analyst* **2012,** *137*, 5885–5890.
59. Hermanson, G. T., Preparation of Colloidal Gold-Labeled Proteins. In *Bioconjugate Techniques*, 2nd ed.; Elsevier Inc.: 2008; pp 924–935.
60. Yun, C. S.; Javier, A.; Jennings, T.; Fisher, M.; Hira, S.; Peterson, S.; Hopkins, B.; Reich, N. O.; Strouse, G. F., Nanometal Surface Energy Transfer in Optical Rulers, Breaking the FRET Barrier, *J. Am. Chem. Soc.* **2005**, *127*, 3115–3119.61. Guddat, L. W.; Herron, J. N.; Edmundson, A. B., Three-dimensional structure of a human immunoglobulin with a hinge deletion. *Proc. Natl. Acad. Sci USA* **1993,** *90*, 4271–4175.
62. Day, R. N.; Davidson, M. W., The fluorescent protein palette: tools for cellular imaging. *Chem. Soc. Rev.* **2009**, *38*, 2887-2921.
63. Remington, S. J.; Wachter, R. M.; Yarbrough, D. K.; Branchaud, B.; Anderson, D. C.; Kallio, K.; Lukyanov, K. A., zFP538, a yellow-fluorescent protein from Zoanthus, contains a novel three-ring chromophore. *Biochemistry* **2005,** *44*, 202–212.

64. Haiss, W.; Thanh, N. T. K.; Aveyard, J.; Fernig, D. G., Determination of Size and Concentration of Gold Nanoparticles from UV-Vis Spectra. *Anal. Chem.* **2007,** *79*, 4215–4221.
65. Aldeek, F.; Safi, M.; Zhan, N.; Palui, G.; Mattoussi, H., Understanding the Self-Assembly of Proteins onto Gold Nanoparticles and Quantum Dots Driven by Metal-Histidine Coordination. *ACS Nano* **2013,** *7*, 10197–10210.
66. Liu, S.; Horak, J.; Höldrich, M.; Lämmerhofer, M., Accurate and Reliable Quantification of the Protein Surface Coverage on Protein-Functionalized Nanoparticles. *Anal. Chim. Acta* **2017,** *989*, 29–37.

FB_1 → low fluorescence

FB_1 → high fluorescence